CERN-ACC-2014-0051

EuCARD-2

Enhanced European Coordination for Accelerator Research & Development

Journal Publication

Radiation-Reaction Trapping of Electrons in Extreme Laser Fields

Ji, L L (Heinrich-Heine-Universität Düsseldorf, Chinese Academy of Sciences) *et al*

08 April 2014

The EuCARD-2 Enhanced European Coordination for Accelerator Research & Development project is co-funded by the partners and the European Commission under Capacities 7th Framework Programme, Grant Agreement 312453.

This work is part of EuCARD-2 Work Package **13: Novel Acceleration Techniques (ANAC2)**.

The electronic version of this EuCARD-2 Publication is available via the EuCARD-2 web site <http://eucard2.web.cern.ch/> or on the CERN Document Server at the following URL: <http://cds.cern.ch/search?p=CERN-ACC-2014-0051>

CERN-ACC-2014-0051

Radiation-Reaction Trapping of Electrons in Extreme Laser Fields

L. L. Ji,[1,2] A. Pukhov,[1] I. Yu. Kostyukov,[3,4] B. F. Shen,[2] and K. Akli[5]
[1]Institut für Theoretische Physik I, Heinrich-Heine-Universität Düsseldorf, 40225 Düsseldorf, Germany
[2]Shanghai Institute of Optics and Fine Mechanics, Chinese Academy of Sciences, Shanghai 201800, China
[3]Institute of Applied Physics of the Russian Academy of Sciences, 603950 Nizhny Novgorod, Russia
[4]Lobachevsky National Research University of Nizhni Novgorod, 603950 Nizhny Novgorod, Russia
[5]The Ohio State University, Columbus, Ohio 43210, USA
(Received 16 December 2013; published 8 April 2014)

A radiation-reaction trapping (RRT) of electrons is revealed in the near-QED regime of laser-plasma interaction. Electrons quivering in laser pulse experience radiation reaction (RR) recoil force by radiating photons. When the laser field reaches the threshold, the RR force becomes significant enough to compensate for the expelling laser ponderomotive force. Then electrons are trapped inside the laser pulse instead of being scattered off transversely and form a dense plasma bunch. The mechanism is demonstrated both by full three-dimensional particle-in-cell simulations using the QED photonic approach and numerical test-particle modeling based on the classical Landau-Lifshitz formula of RR force. Furthermore, the proposed analysis shows that the threshold of laser field amplitude for RRT is approximately the cubic root of laser wavelength over classical electron radius. Because of the pinching effect of the trapped electron bunch, the required laser intensity for RRT can be further reduced.

DOI: 10.1103/PhysRevLett.112.145003 PACS numbers: 52.27.Ny, 52.38.Ph, 52.65.Rr

Laser intensities up to 10^{22} W/cm^2 have been demonstrated [1] and are expected to surpass 10^{23} W/cm^2 in the course of several ongoing projects and initiatives [2,3]. At this intensity level, the laser-plasma interaction will be prompted to the exotic near-QED regime [4–10]. A most foreseeable effect is that electrons lose a considerable amount of energy by emitting photons in the laser field, namely the radiation reaction (RR) effect [11]. Particle-in-cell (PIC) simulations suggest that γ photons may become the dominant energy absorption channel and even take more energy than electrons [7–9]. As a result, the relativistic motion of electrons at these laser intensities is strongly modified [12,13]. It leads to much lower electron energies than the ones one would expect neglecting RR [14–23]. It has also been noticed that free electrons can be attracted to the positions of electric field peaks in the near-QED regime by creating a standing wave structure with multiple lasers [24–26].

Nevertheless, the knowledge about the multidimensional features of laser-plasma interaction in the QED-dominated regime is still limited. In a non-QED regime, the laser ponderomotive force expels electrons off the high-intensity regions. An electron-free channel or a bubble is usually formed depending on the plasma density and pulse duration. Yet, in the QED regime, when the RR effect dominates, the collective electron response and laser propagation dynamics remain unclear.

In this Letter, we investigate the laser-plasma interaction in the near-QED regime via full three-dimensional (3D) PIC simulations. We found radiation-reaction trapping (RRT) of a dense electron bunch inside the laser pulse. When a sufficiently intense laser propagates in plasma, we observe a new regime, where the RR force can compensate for the ponderomotive force. Unlike in the non-QED regime, electrons can be transversely trapped by the laser field instead of being pushed away. Different from the standing EM wave cases [24–26], where electrons are mostly confined in a small volume of the laser wavelength, a traveling wave is considered here. The spatial period and the oscillation amplitude are typically large as compared with the laser wavelength. As we see later, the RR reduces oscillation amplitude, leading to a concentration of electrons in the high-intensity region and forming of a dense bunch. Since the bunch becomes ultrarelativistic quickly and copropagates with the laser, the electric part of the transverse Lorentz force is almost compensated by the magnetic part. The required laser amplitude for RRT is then greatly reduced. The RRT changes the laser-plasma interaction significantly. Furthermore, a large part of the laser energy is converted into high-energy photons providing a bright source of MeV γ rays.

The new effect is observed with the code VLPL [27]. A QED model is implemented to describe the RR and electron-positron pair creation [28]. Since we observed an insignificant number of the positrons in the investigated parameter region, the pair creation is not discussed here. We start with linearly polarized (LP) laser pulses, having a profile of $a = a_0 \sin^2(\pi t/2\tau_0) e^{-r^2/r_0^2} \sin(\omega_0 t)$, where ω_0 is the laser angular frequency and $a = eE_L/m_e\omega_0 c$ is the normalized amplitude of laser field, respectively; e and m_e are electron charge and mass. The pulse has a duration of $\tau_0 = 20T_0$ (T_0 is the laser period) and a spot size $r_0 = 5\lambda_0$

 © 2014 American Physical Society

(laser wavelength $\lambda_0 = 0.8\ \mu$m). The simulation box is $60\lambda_0 \times 16\lambda_0 \times 16\lambda_0$ in $X \times Y \times Z$ directions, with a cell size of $0.05\lambda_0 \times 0.25\lambda_0 \times 0.25\lambda_0$, respectively. The laser is polarized along the Y direction and propagates along the X direction. The hydrogen target is a slab located between $35\lambda_0$ to $100\lambda_0$ where we put eight macroparticles per cell initially.

We conduct two simulations with and without RR, respectively. We choose $a_0 = 500$ ($I_0 \approx 5.4 \times 10^{23}$ W/cm^2) and an initial target density $n_e = 20n_c$, where $n_c = m_e\omega_0^2/4\pi e^2$ is the critical electron density. The simulation results are presented in Fig. 1. Frames (a) and (d) show the electron density in the X-Y plane for simulations without and with RR, respectively. The initially overdense target becomes relativistically transparent in both cases. As the ultraintense laser propagates in the plasma, electrons quivering in the laser field experience strong ponderomotive force longitudinally and transversely. Without RR, electrons are mostly expelled from the high-intensity region and pile up at the interface, forming a dense boundary. An evacuated channel is seen in Fig. 1(a), which is filled with the laser radiation.

The interaction is dramatically modified when the RR is switched on. A dense electron bunch appears inside the laser pulse in the channel in Fig. 1(d). Apparently, the RR leads to electron trapping inside the laser. Instead of being swept away by the ponderomotive pressure, electrons escape from the boundary, gradually accumulate at the high-intensity region, and then are constantly confined around the propagation axis. As a consequence, a bunch is formed with a high peak density. The bunch has a length of $\sim 8\lambda_0$. It is confined at the laser axis with a transverse radius of $\sim 3\lambda_0$, roughly defined by the excursion radius in the laser field. The bunch oscillating in the laser field shows a periodic structure with a spatial period of the laser wavelength. Because of the transverse electric field created by

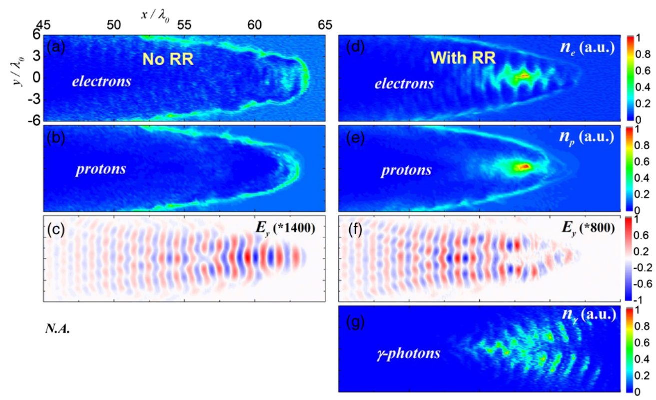

FIG. 1 (color online). Distributions of electron and proton densities and of laser field E_y in the X-Y plane ($z = 0$) at $t = 80T_0$ without RR (a)-(c) and with RR (d)-(f), respectively. The density distribution of emitted γ photons (>1 MeV) is shown in (g). Laser-plasma parameters are $a_0 = 500$, $\tau_0 = 20T_0$, and $n_e = 20n_c$.

trapped electrons, protons also pinch at the axis, forming together a quasineutral relativistic plasma bunch [see in Fig. 1(e)].

This compact plasma bunch consumes most of the laser energy. Comparing the laser field in Fig. 1(f) to the one without RR in Fig. 1(c), one notices that the peak laser amplitude is reduced by nearly 50% with RR. At $t = 80T_0$, about 32.5% of the laser energy is absorbed without RR. When RR is switched on, it is enhanced to 48%. Since electrons are trapped in the most intense region of the laser pulse, they experience the strongest laser field initially. They continuously deplete the laser energy by radiating energetic γ photons and finally create a local "hole" inside the pulse, as shown in Fig. 1(f). This effect leads to the laser ponderomotive force directed to the propagation axis, which helps to confine the bunch more. The bunch begins to expand only when laser energy has been greatly depleted by the plasma. In the simulation, around 35% of the laser energy is converted to tens-of-MeV photons after the laser is fully depleted providing an efficient γ-ray source.

The density distribution of photons in the X-Y plane is presented in Fig. 1(g). Apparently, the photons originating from the electron bunch depart in two primary directions, showing a two-jet structure. Photons are emitted preferentially at a certain angle with respect to the propagating direction. This means that the electrons acquire not only longitudinal but also transverse recoil forces, and it is this transverse recoil that leads to the confinement of electrons.

The new RRT effect stems from RR, and electrons are transversely trapped by the laser pulse when the RR force is comparable to the laser ponderomotive force. The underlying mechanism is shown in Fig. 2(a). Electrons quivering in the highly relativistic laser field emit photons along their propagation directions, causing a recoil force oppositely directed to the instantaneous momentum [31]. The tendency of the laser ponderomotive force to push electrons forward and aside is compensated by the recoil force. In the limit of strong RR, the recoil can be so strong that instead of being expelled away, electrons gradually fall into the high-laser-intensity region and are trapped there.

In the regime of RRT, photons are emitted at an angle with respect to the propagation direction, providing the transverse recoil force. This has been partially proven in Fig. 1(g). We show the corresponding angular distribution of high-energy photons (>1 MeV) in the 3D domain in Fig. 2(b). Here θ is defined as the included angle between the X direction and the photon momentum, and φ is the angle between the Y axis and the transverse photon momentum. The photons are preferentially emitted in the polarization plane (intensity peaks at $\varphi = 0°, 180°$). The distribution peaks at $\theta \approx 15°$ and stretches up to $\theta \approx 30°$. This clearly demonstrates the off-axis radiation of trapped electrons. Because of momentum conservation, the outward-moving photons induce inward recoil to the oscillating electrons and hence a confining force. This recoil force is the origin of RRT. Several mechanisms of γ-ray generation are proposed for relativistically transparent regimes of laser-plasma interaction (see, for example, [29,30]), which predict similar characteristics of γ photons. In real experimental situations, a combination of many mechanisms may be responsible for γ-ray generation, and further investigations are needed to classify the regimes of interaction.

In the following, we show from analysis that RRT appears in the limit of strong RR. Taking into account the RR force in the Landau-Lifshitz form [31], the motion of a free electron in a laser field is

$$\frac{d\mathbf{p}}{dt} = \mathbf{F}_L + \mathbf{F}_{rr}, \qquad (1)$$

where $\mathbf{F}_L = -e(\mathbf{E} + \mathbf{v} \times \mathbf{B}/c)$ is the Lorentz force and $\mathbf{F}_{rr} \approx -(2e^4/3m_e^2c^5)\gamma^2\mathbf{v}[(\mathbf{E} + \mathbf{v} \times \mathbf{B}/c)^2 - (\mathbf{E}\cdot\mathbf{v})^2/c^2]$ is the RR force. We keep only the main term proportional to γ^2 in the strong relativistic case. Here $\mathbf{E}$ and $\mathbf{B}$ are the electric and magnetic field of the laser, and the electron momentum is $\mathbf{p} = \gamma m_e \mathbf{v}$. The trajectory of a test electron can be obtained numerically by solving Eq. (1), using a specific laser field.

To demonstrate the RRT effect, we follow trajectories of test electrons in a laser pulse in vacuum. We assume the normalized electric field E_y of the LP pulse to have the profile$E_y = a\cos(k_p y)\cos(k_p z)\sin(k_x x - t)$, where $a = a_0 e^{-(x-t)^2/\tau^2}$ is the temporal profile. Here $k_p = \pi/2r_0$ is the perpendicular wave number; hence, $\mathbf{E} = \mathbf{B} = 0$ for $|y|, |z| \geq r_0$. For simplicity, we normalize time to ω_0^{-1}, length to c/ω_0, wave number k to ω_0/c, and momentum to $m_e c$, respectively. Other field components are calculated according to the Maxwell equations in vacuum: $E_x = 0$, $E_z = a\sin(k_p y)\sin(k_p z)\sin(k_x x - t)$, $B_x = -2ak_p\cos(k_p y)\sin(k_p z)\cos(k_x x - t)$, $B_y = -k_x E_z$, and $B_z = k_x E_y$, where $k_x^2 + 2k_p^2 = 1$. The 3D trajectories of electrons initially located inside the laser pulse ($\lambda_0 = 1\ \mu$m, $a_0 = 900$, $r_0 = 8\lambda_0/2\pi$, $\tau = 100T_0/2\pi$) are numerically calculated first with RR switched off and then on. The results are shown in Fig. 2(a). Without RR, electrons oscillate in the laser field for a short period and then are scattered. On the contrary, when including the RR, a significant part of electrons is confined close to the axis. This is due to the emission of γ photons at considerable angles.

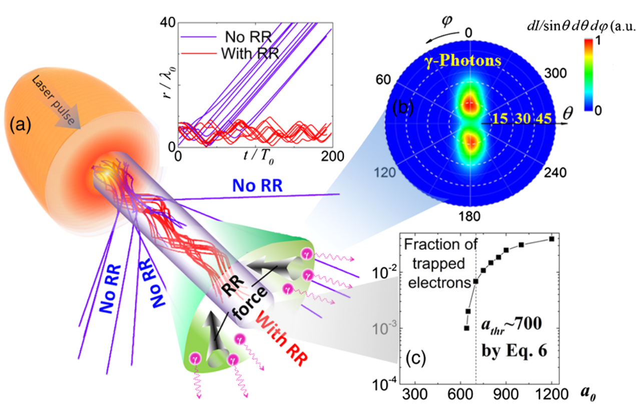

FIG. 2 (color online). Sketch of laser-plasma interaction in the regime of RRT. (a) Trajectories of test electrons numerically calculated according to Eq. (1) either neglecting (blue solid lines) or including RR (red solid lines). Electrons are trapped in the high-laser-intensity region through the RR force (black arrow) induced by the emitted photons (wavy arrows). The upper panel shows the corresponding distance $r = \sqrt{y^2 + z^2}$ of the electrons away from the propagation axis versus time. (b) The typical angular distribution of γ photons from 3D PIC simulations. (c) The relative fraction of trapped test electrons versus laser amplitude.

RRT appears when the laser amplitude reaches some threshold so that the RR becomes strong enough to compensate for the Lorentz force. To simplify the analysis of the critical condition, we work in two-dimensional (2D) geometry below as the pulse is polarized in the X-Y plane. Assuming that the electron undergoes transverse oscillations around the propagation direction X, we introduce the following quantities: $t_{p,n}$ and y_n are the moments and transverse coordinates of the electron when its transverse momentum vanishes $p_y = 0$; $t_{y,n}$ and $p_{y,n}$ are the moments and transverse electron momentum when $y = 0$. Thus, y_n characterizes the transverse oscillation amplitude. For definiteness, we assume that $y_{2n-1} > 0$ and $y_{2n} < 0$, where $n = 1, 2, 3, \ldots$. The equation of electron transverse momentum is

$$p_y(t) = \int_{t_{p,n-1}}^{t} F_{L,y}(t')dt' - \frac{v_y(t_{y,n})}{|v_y(t_{y,n})|}\int_{t_{p,n-1}}^{t} F_{rr,y}(t')dt', \qquad (2)$$

where $F_{L,y} = -e(E_y - v_x B_z/c)$ and $F_{rr,y} = (v_y/\mathbf{v})\mathbf{F}_{rr}$ are the y components of the Lorentz force and the RR force, respectively. Noticing that the sign of the first term in Eq. (2) coincides with that of $v_y(t_{y,n})$, the oscillating amplitude can be written as

$$|y_n| = \left|\int_{t_{y,n}}^{t_{p,n}} \frac{dt}{m_e c\gamma(t)}\int_{t_{p,n-1}}^{t} dt' F_{L,y}(t')\right| - \left|\int_{t_{y,n}}^{t_{p,n}} \frac{dt}{m_e c\gamma(t)}\int_{t_{p,n-1}}^{t} dt' F_{rr,y}(t')\right|. \qquad (3)$$

Apparently RR reduces the electron excursion in the transverse direction and improves the transverse confinement of the electron.

According to Eq. (3), the critical condition can be estimated when $F_{L,y} \sim F_{rr,y}$. In 2D, the laser field is simplified to $E_y = a_0\cos(k_p y)\sin(k_x x - t)$, where the temporal profile is neglected since we focus on the transverse confinement. For an electron under an ultrarelativistic laser, the hierarchy of inequalities can be assumed $\gamma \approx p_x \gg p_y \gg 1$ and $k_x \gg k_p > v_y$. Hence,

$$k_x x - t = (k_x v_x - 1)t \approx \left[\left(1 - k_p^2/2\right)\left(1 - v_y^2/2\right) - 1\right]t \equiv -\Omega t, \tag{4}$$

where $\Omega \approx k_p^2/2 + v_y^2/2 \approx k_p^2/2$. The Lorentz force turns out to be $F_{L,x} \sim ak_p \cos \Omega t$ and $F_{L,y} \sim (1/2)ak_p^2 \sin \Omega t$, while the related RR force is estimated as $F_{rr,x} \sim (2\omega_0 r_e/3c)a^4/k_p^2$ and $F_{rr,y} \sim (2\omega_0 r_e/3c)a^4/k_p^3$, where $r_e = e^2/m_e c^2$ is the classical electron radius. The threshold of laser amplitude is obtained by demanding $F_{L,x} \sim F_{rr,x}$, $F_{L,y} \sim F_{rr,y}$, or both. They both give the same critical condition:

$$a_{thr} \sim (2k_p \omega_0 r_e/3c)^{-1/3} \sim (r_0/r_e)^{1/3}. \tag{5}$$

Here the laser focal spot radius r_0 is of a few laser wavelengths. Equation (5) reveals explicitly that the threshold is at the order of the cubic root of laser wavelength over the classical electron radius $a_{thr} \sim 700$. It shows a rather weak dependence on the laser wavelength.

The free electron analysis suggests that RRT could be achieved when $a_0 \geq a_{thr}$. In our 3D test-particle simulations based on Eq. (1), we simulated an ensemble of electrons uniformly distributed over one laser period within the focal spot. Then we calculated the fraction of electrons that remained trapped. Figure 2(c) clearly shows that the electron trapping starts when the laser amplitude approaches $a_{thr} \sim 700$, in good agreement with our prediction.

A further demonstration of the hypothesis is performed with 3D PIC simulations by scanning over laser amplitudes, from $a_0 = 50$ to $a_0 = 700$ at the target density of $n_H = n_e = 10n_c$. This target is relativistically transparent to all of the employed pulses, and the laser spot size is fixed at $r_0 = 3\lambda_0$.

The energies deposited to electrons and photons divided by the total laser energy (defined as the conversion efficiency η) as a function of the laser amplitude are shown in Fig. 3(a). At low intensities, electrons carry as much as 40% of laser energy, while photons hardly take away any. As a_0 increases, the photon emission and the RR grow. The energy conversion efficiency for electrons η_e drops, while the one for photons η_γ rises accordingly. When it reaches $a_0 = 300$, both electrons and photons obtain about 15% energy from the laser. Beyond this critical amplitude, γ photons acquire more laser energy than electrons.

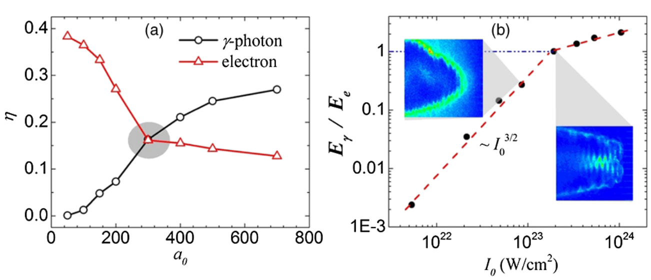

FIG. 3 (color online). Energies absorbed by electrons and γ photons divided by the total laser energy versus laser amplitude (a); total energy of γ photons over that of electrons as a function of laser intensity (b). The inner panels show the electron density distribution at $a_0 = 200\,(\sim 10^{23}\ \mathrm{W/cm^2})$ and $a_0 = 300(\sim 2 \times 10^{23}\ \mathrm{W/cm^2})$, respectively.

The domination of γ photons as the superior energy conversion channel over electrons marks the point where the RRT emerges. We plot the total energy of photons E_γ over that of electrons E_e for different laser intensities in Fig. 3(b). We start to observe RRT when $E_\gamma/E_e \geq 1$, or $I_0 \geq 2 \times 10^{23}\ \mathrm{W/cm^2}$. The insets in Fig. 3(b) show characteristic electron density distributions slightly below the threshold (no RRT) and slightly above it (RRT). The energy partitions in different regimes can be interpreted from the momentum conservation law. The momentum of a photon is related to its energy $p_\gamma = \varepsilon_\gamma/c$. For highly relativistic electrons, the relation $p_e \approx \varepsilon_e/c$ holds as well. Hence, when electrons radiate photons with total energy comparable to themselves ($\eta_\gamma = \eta_e$), the total momenta of both species equal each other $\sum p_\gamma \approx \sum p_e$. It means that the electron momenta can be properly balanced by the recoil of photon momenta as photons are always emitted in the opposite directions of the electron momenta, and RRT appears.

The critical condition $\eta_\gamma = \eta_e$ distinguishes two different regions in Fig. 3(b), which shows different scaling laws for the energy ratio between photons and electrons. It is known that the power of synchrotron radiation is proportional to γ_e^4, where γ_e is the relativistic factor of the radiating electron. Hence, $E_\gamma/E_e \sim \gamma_e^3$. In the non-RRT regime, the RR effect is just a perturbation so that the averaged electron energy is approximately $\bar{\gamma}_e \sim a_0$ giving the power law of $E_\gamma/E_e \sim I_0^{3/2}$ (see in Fig. 3b) [8]. As it enters the RRT regime, the power law saturates.

The required laser amplitude for RRT in simulations is lower than the one predicted by the free-electron analysis because of the collective plasma effects. As shown in Fig. 1, the electron cloud copropagates with the laser pulse nearly at the speed of light, generating an extraordinary current. Background protons are dragged by the induced charge separation field. They attempt to catch up with electrons at a much lower velocity, around $0.65c$, as shown in Fig. 4(a). The electron bunch carries a total charge of around 600 nC. The total current taking into account the compensation of ion current is about 1.4×10^7 A, building up a strong poloidal magnetic field of peak value 1.2×10^{10} G. This reaches 20% of the peak laser magnetic field, as shown in Fig. 4(b). Such a strong poloidal magnetic field leads to a significant pinching effect on the propagating bunch.

Seeded by the RR force and enhanced by the pinching effect, the dense electron bunch is confined inside the

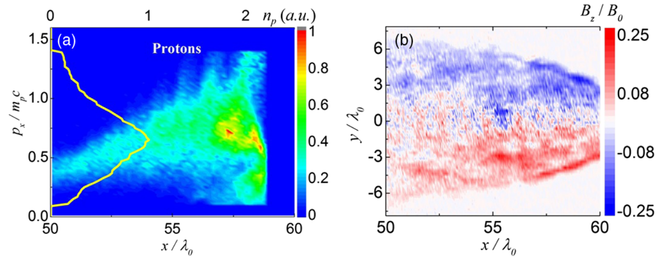

FIG. 4 (color online). (a) Phase space distribution of protons ($x - p_x$) for $a_0 = 500$ and $n_H = n_e = 20n_c$ at $t = 80T_0$. (b) The self-generated magnetic field B_z in the X-Y plane is taken along the laser axis.

driving laser during the whole interaction. For $n_e = 20n_c$, the critical laser amplitude of RRT in simulations is reduced significantly as compared to the threshold from analysis. Thus the new effect may be observed with the foreseen laser pulses ($\sim 10^{23}$ W/cm^2) in the near future. A most interesting consequence induced by RRT is the enhanced emission of photons. The confined electrons quiver directly in the most intense part of the laser field, absorb most of the laser energy immediately, and radiate energetic photons at high efficiencies. In Fig. 3(a), the laser-to-photon conversion efficiency is above 20% in the RRT regime.

To conclude, a new trapping effect of electrons inside the laser pulse is discovered in the near QED regime. The oscillation amplitude of electrons in the laser pulse strongly declines due to RR. Plenty of electrons gather around the propagating axis and form a dense bunch through the pinching effect. RRT leads to a collimated high-density plasma bulk inside the laser pulse such that γ-photon emission is greatly enhanced.

L. L. J. acknowledges the support from the Alexander von Humboldt Foundation. This work is also supported by the National Natural Science Foundation of China (Projects No. 11125526, No. 11335013, and No. 11374317). K. A. is supported by the AFOSR Young Investigator Program (YIP) under Contract No. FA9550-12-1-0341. This work is also supported by the Government of the Russian Federation (Project No. 14.B25.31.0008) and by the Russian Foundation for Basic Research (Grants No. 13-02-00886 and No. 13-02-97025) and by EU FP7 Eucard-2.

[1] V. Yanovsky *et al.*, Opt. Express **16**, 2109 (2008).
[2] Extreme Light Infrastructure European Project, www.eli-laser.eu.
[3] Exawatt Center for Extreme Light Studies, www.xcels.iapras.ru.
[4] A. M. Fedotov, N. B. Narozhny, G. Mourou, and G. Korn, Phys. Rev. Lett. **105**, 080402 (2010).
[5] A. Di Piazza, C. Müller, K. Z. Hatsagortsyan, and C. H. Keitel, Rev. Mod. Phys. **84**, 1177 (2012).
[6] I. V. Sokolov, J. A. Nees, V. P. Yanovsky, N. M. Naumova, and G. A. Mourou, Phys. Rev. E **81**, 036412 (2010).
[7] C. P. Ridgers, C. S. Brady, R. Duclous, J. G. Kirk, K. Bennett, T. D. Arber, and A. R. Bell, Phys. Plasmas **20**, 056701 (2013).
[8] E. N. Nerush *et al.*, arXiv:1309.1648.
[9] L. L. Ji, A. Pukhov, E. N. Nerush, I. Yu. Kostyukov, B. F. Shen, and K. U. Akli, Phys. Plasmas **21**, 023109 (2014).
[10] E. N. Nerush, I. Yu. Kostyukov, A. M. Fedotov, N. B. Narozhny, N. V. Elkina, and H. Ruhl, Phys. Rev. Lett. **106**, 035001 (2011).
[11] Ya. B. Zel'dovich, Sov. Phys. Usp. **18**, 79 (1975).
[12] N. Neitz and A. Di Piazza, Phys. Rev. Lett. **111**, 054802 (2013).
[13] R. T. Hammond, Electron. J. Theor. Phys. **7**, 221 (2010).
[14] A. Zhidkov, J. Koga, A. Sasaki, and M. Uesaka, Phys. Rev. Lett. **88**, 185002 (2002).
[15] A. Di Piazza, K. Hatsagortsyan, and C. Keitel, Phys. Rev. Lett. **102**, 254802 (2009).
[16] M. Tamburini, T. V. Liseykina, F. Pegoraro, and A. Macchi, Phys. Rev. E **85**, 016407 (2012).
[17] R. Capdessus, E. d'Humières, and V. T. Tikhonchuk, Phys. Rev. E **86**, 036401 (2012).
[18] S. V. Bulanov *et al.*, arXiv:1304.6519v1.
[19] M. Chen, A. Pukhov, T. P. Yu, and Z. M. Sheng, Plasma Phys. Controlled Fusion **53**, 014004 (2011).
[20] I. V. Sokolov, N. M. Naumova, J. A. Nees, G. A. Mourou, and V. P. Yanovsky, Phys. Plasmas **16**, 093115 (2009).
[21] N. Naumova, T. Schlegel, V. Tikhonchuk, C. Labaune, I. Sokolov, and G. Mourou, Phys. Rev. Lett. **102**, 025002 (2009).
[22] I. Kostyukov, S. Kiselev, and A. Pukhov, Phys. Plasmas **10**, 4818 (2003).
[23] R. Capdessus, E. d'Humières, and V. T. Tikhonchuk, Phys. Rev. Lett. **110**, 215003 (2013).
[24] G. Lehmann, and K. H. Spatschek, Phys. Rev. E **85** 056412 (2012).
[25] J. G. Kirk, A. R. Bell, and I. Arka, Plasma Phys. Controlled Fusion **51**, 085008 (2009).
[26] A. Gonoskov *et al.*, arXiv:1306.5734v2.
[27] A. Pukhov, J. Plasma Phys. **61**, 425 (1999).
[28] A. M. Pukhov and I. Yu. Kostyukov, Probl. At. Sci. Technol. **4**, 245 (2013).
[29] T. Nakamura, J. K. Koga, T. Zh. Esirkepov, M. Kando, G. Korn, and S. V. Bulanov, Phys. Rev. Lett. **108**, 195001 (2012).
[30] C. S. Brady, C. P. Ridgers, T. D. Arber, and A. R. Bell, Plasma Phys. Controlled Fusion **55**, 124016 (2013).
[31] L. D. Landau and E. M. Lifshitz, *The Classical Theory of Fields*, A Course of Theoretical Physics (Pergamon Press, Oxford, 1971), Vol. 2.